J. Fluid Mech. (1990), *vol.* 214, *pp.* 559–578
Printed in Great Britain

Three-dimensional numerical simulation of buoyancy-driven convection in vertical cylinders heated from below

By G. NEUMANN†

Institut für Werkstoffwissenschaften VI, Universität Erlangen-Nürnberg, Martensstraße 7, D-8520 Erlangen, FRG

(Received 16 November 1987 and in revised form 30 October 1989)

Steady and oscillatory convection in rigid vertical cylinders heated from below is studied by means of a numerical solution of the three-dimensional, time-dependent Boussinesq equations. Both adiabatic and ideal conducting sidewalls are considered. The effect of the geometry of the container on the onset of convective instability and the structure and symmetry of the flow are analysed and compared with the results of linear stability theories. The nonlinear evolution and stability of convective flows at Rayleigh numbers beyond the critical number for the onset of convective motion are investigated for Prandtl numbers of 0.02 to 6.7. The limits of stable axisymmetric solutions are an important finding of this study. The onset and the frequency of oscillatory instability are calculated for the small Prandtl number 0.02 and compared with experimental data. Calculated stream patterns and velocity profiles illustrate the three-dimensional structure of steady convection and the time-dependent behaviour of oscillatory flows.

1. Introduction

In recent years there has been an increasing interest in improving the quality of bulk single-crystal semiconductor materials required by the micro-electronics industry. The performance of electronic devices often depends strongly on the compositional homogeneity of the substrates upon which they are fabricated.

It has been well known for about twenty years that convective motion in the melt plays an important role in determining heat and mass transfer during solidification processes (Müller 1988). Hence, a detailed understanding of the fluid flow in crystal growth configurations has become important.

Since the experiments of Bénard (1900) the analysis of buoyancy-driven flows in fluid layers heated from below (Rayleigh–Bénard convection) has been the aim of numerous theoretical and experimental studies. Such fundamental aspects as the onset of convective instability, transitions to periodic and non-periodic motions, and the influence of boundary and initial conditions have been investigated. More recently attention has been focused on the effect of rigid lateral boundaries on the stability and form of the convective motion; in particular, rectangular and cylindrical geometries have been investigated. A wide range of values for the physical parameters has been studied in parallelepipeds and, mostly flat, cylindrical containers.

† Present address: Fraunhofer-Institut für Angewandte Festkörperphysik, Eckerstraße 4, D-7800 Freiburg, FRG.

Only a few results can be applied to the most important vertical crystal growth techniques, such as the Czochralski, vertical Bridgman or zone-melting techniques. Therefore the main purpose of the present numerical analysis is to investigate convection in vertical cylinders with large or moderate aspect ratios (a = height/diameter), where lateral confinement has an important influence. For geometries with imposed temperature fields that are purely vertical and heated from below, steady convection begins at a critical temperature difference, measured in terms of the Rayleigh number, beyond which the static fluid is unstable to small-amplitude disturbances of the velocity, pressure and temperature fields. These critical Rayleigh numbers ($R_{c,s}$) are determined as the eigenvalues for marginal stability in an analysis constructed from the Boussinesq equations (§2) linearized about the static state (Chandrasekhar 1961). Critical Rayleigh numbers for the onset of convection in vertical cylinders with rigid walls have previously been calculated by Charlson & Sani (1971), Gershuni & Zhukhovitskii (1976) and Buell & Catton (1983). In the above studies it is further predicted that convection in rigid cylinders sets in as an axisymmetric mode only for flat containers, whereas for aspect ratios greater one convection is always non-axisymmetric. For non-rigid or combinations of rigid and non-rigid walls the linear stability problem can be solved analytically by the separation of variables as shown by Zierep (1963), Catton & Edwards (1967) and Rosenblat (1982). The exact solutions are used for testing the accuracy of the numerical procedure developed in this work (§3.2).

The calculation of fluid motions that evolve for Rayleigh numbers beyond the critical values ($R_{c,s}$) requires nonlinear analysis, either by perturbation methods (Schlüter, Lortz & Busse 1965) or by numerical solution of the full Boussinesq equations. Perturbation techniques are valid only in cases where the Rayleigh numbers are still close to the critical value. Numerical calculations have the potential for determining fluid flows over a much wider range of Rayleigh numbers and for describing the nonlinear evolution of the flow structure with changes in the geometry of the cavity, the Prandtl number or the thermal boundary conditions. This paper describes such a three-dimensional numerical study of convection in rigid vertical cylindrical enclosures (§4, 5).

Beyond various aspects of fundamental interest, investigations of the nonlinear evolution of convection, and especially of stability boundaries and changes in the symmetry of the flow, are very important for the design and optimization of crystal growth apparatus.

2. Physical and mathematical model

We consider a fluid layer in a vertical cylindrical enclosure of height h and diameter d. A Newtonian fluid with constant kinematic viscosity ν and thermal diffusivity κ, and whose density ρ varies linearly with temperature is assumed (Boussinesq approximation). The two ends of the cylinder are taken to be isothermal with the lower one held at temperature T_b, which is greater than the temperature T_a of the upper surface. A cylindrical coordinate system $\boldsymbol{r} = (r, \theta, z)$ with its origin at the centre of the lower boundary is employed. The equations that govern the temperature $T(\boldsymbol{r}, t)$, pressure $p(\boldsymbol{r}, t)$ and velocity $\boldsymbol{v}(\boldsymbol{r}, t) = (v_r, v_\theta, v_z)$ fields are the conservation equations for mass (continuity equation), momentum (Navier–Stokes equations) and energy, called the Boussinesq equations (Chandrasekhar 1961). By scaling length with the height h of the cylinder, velocity with κ/h, pressure with $\rho\kappa^2/h^2$, time with

h^2/κ and temperature T as $(T-T_a)/(T_b-T_a)$ the Boussinesq equations can be written in dimensionless form as

$$\nabla \cdot \boldsymbol{v} = 0, \tag{1a}$$

$$\partial \boldsymbol{v}/\partial t + \boldsymbol{v} \cdot \nabla \boldsymbol{v} = -\nabla p + P\nabla^2 \boldsymbol{v} + RPT\boldsymbol{e}_z, \tag{1b}$$

$$\partial T/\partial t + \boldsymbol{v} \cdot \nabla T = \nabla^2 T, \tag{1c}$$

where $\boldsymbol{e}_z$ is the unit vector in the vertical upward direction.

The dimensionless Rayleigh number R and Prandtl number P in (1) are defined as

$$R = g\alpha h^3(T_b-T_a)/\nu\kappa, \tag{2}$$

$$P = \nu/\kappa, \tag{3}$$

where α and g are the coefficient of thermal expansion and the acceleration due to gravity, respectively.

At all container walls either the no-slip or the shear-free velocity boundary condition is prescribed. The cylindrical sidewall is chosen to be adiabatic or ideal conducting, i.e. the temperature gradient normal to the wall is set equal to zero or the temperature of the sidewall varies linearly from T_b to T_a. For either set of boundary conditions the entire set has the static solution

$$\boldsymbol{v} = 0, \quad T(z) = 1-z, \quad p = p_0 + RP(z-\tfrac{1}{2}z^2), \tag{4}$$

from which the convective motions branch. We shall represent these flows by the Nusselt number

$$N = \frac{4a^2}{\pi}\int_0^{2\pi}\int_0^{\frac{1}{2a}} r\left(-\frac{\partial T}{\partial z}\bigg|_{z=0,1}\right)\mathrm{d}r\,\mathrm{d}\theta, \tag{5}$$

where $a = h/d$ is the aspect ratio. The temperature gradient $\partial T/\partial z$ is evaluated either along the top end ($z = 1$) or the bottom end ($z = 0$) of the cylinder.

3. Numerical solution

3.1. *Numerical method*

To render (1) in a format suitable for computation, they are expressed in finite-difference form on a three-dimensional cylindrical mesh. The region in which the computations are to be performed is divided into a set of small cells having edge length Δr, $r\Delta\theta$ and Δz. An appropriately staggered mesh (Harlow & Welch 1965; Williams 1969) is used for the solution of the Navier–Stokes equations. In each cell the velocity components are defined at the cell faces while the values of pressure and temperature apply to the centre of the cell (figure 1).

The numerical computations are performed by an *implicit finite-difference method* using first-order forward differences for the derivatives in time and second-order central differences for the spatial derivatives. For a velocity field with zero divergence the nonlinear and the diffusive terms in (1) can be written in an equivalent form:

$$\nabla^2 \boldsymbol{v} = -\nabla \times (\nabla \times \boldsymbol{v}), \tag{6a}$$

$$\boldsymbol{v} \cdot (\nabla \boldsymbol{v}) = \tfrac{1}{2}[\boldsymbol{v} \cdot (\nabla \boldsymbol{v}) + \nabla(\boldsymbol{v} \cdot \boldsymbol{v})], \tag{6b}$$

$$\boldsymbol{v} \cdot (\nabla T) = \tfrac{1}{2}[\boldsymbol{v} \cdot (\nabla T) + \nabla(\boldsymbol{v}T)]. \tag{6c}$$

As proposed by Williams (1969) and Piacsek & Williams (1970) for the conservation properties of numerical schemes, the finite-difference analogue of the right-hand side of (6) is used.

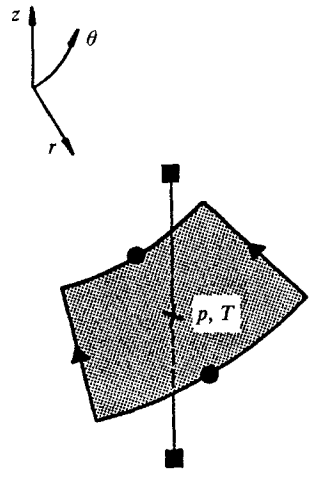

FIGURE 1. Computational mesh. Position of the staggered mesh points within one cell: ×, pressure and temperature; ▲, azimuthal, ●, radial, and ■, vertical velocity points.

A time-dependent solution is obtained as follows. At time $t = 0$ we start with the initial conditions for the velocity and temperature fields. In the first stage we advance the velocity and temperature components from the previous state at $t = t_n$ to the new state at time $t = t_n + \Delta t$. The implicitly coupled finite-difference equations are solved iteratively by the *Alternating-Direction-Implicit* method of Douglas & Gunn (1964). This method leads to the solution of tridiagonal and cyclic-tridiagonal matrices which can easily be solved by Gauss elimination. However, this procedure does not lead to a velocity field with zero divergence, i.e. the continuity equation (1*a*) is not fulfilled. Thus, in a second stage, the velocity and pressure components in each cell have to be corrected in such a way that zero divergence is approached. After this one advances to the next time step ($t = t_{n+1}$).

The so-called SIMPLE algorithm of Patankar (1980) is applied for the correction of the velocity and pressure components. Since zero divergence cannot be reached after one correction step, the procedure has to be performed iteratively until all cells have attained a suitably small divergence. The values for the correction of the pressure and velocity fields are calculated by solving a second-order Poisson equation for the pressure at each correction step.

The whole numerical algorithm is written serially as well as in vectorized form for the calculation on CRAY-1 computers. Run times are presented for the example of a three-dimensional oscillatory solution (§5). Additionally, an axisymmetric version of the algorithm is available. For more details on the numerical scheme see Neumann (1986).

3.2. *Test of the numerical scheme*

Analytical solutions obtained for vertical cylindrical containers with free surfaces (see Rosenblat 1982) are compared with the corresponding numerical ones in order to test the accuracy of the numerical method. In order to limit computer costs only *axisymmetric* solutions (azimuthal wavenumber $m = 0$, i.e. flows being purely meridional and independent of the azimuth θ) are presented in this section. Analytical solutions derived by Rosenblat (1982) for the onset of convection in cylinders with the shear-free velocity boundary condition† and adiabatic sidewalls

† It should be noted that for the case of axisymmetric solutions (with $v_\theta = 0$) presented in this section, the two kinds of boundary conditions at the curved cylinder wall, shear-free and zero tangential vorticity, are identical.

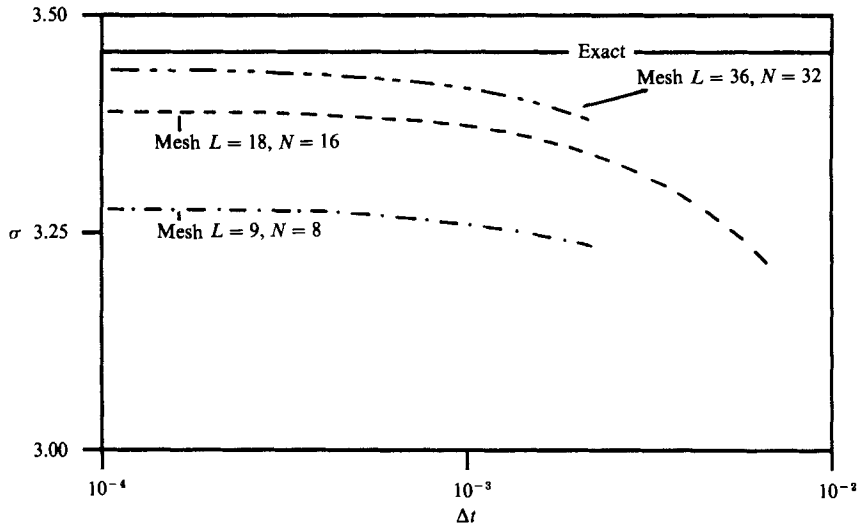

FIGURE 2. Growth exponents σ of axisymmetric convection in a shear-free cylinder in dependence on the spatial and temporal discretization for $a = 0.2899$, adiabatic sidewall, $R = 1000$ and $P = 1$. Comparison with the exact analytical value (equation (7)). L and N denote the number of mesh points in the radial and vertical directions.

Aspect ratio, a	$R_{c,s}$ analytical	$R_{c,s}$ numerical, $\sigma \to 0$	Error
0.2899	657.51	659	0.2%
0.21	735.41	737	0.2%

TABLE 1. Comparison of critical Rayleigh numbers for the onset of axisymmetric convection in shear-free cylinders obtained by extrapolation with the exact analytical values

are taken for the comparison with the numerical computations. As is known from linear stability analysis an exponential time law $u = u_0 \exp(\sigma t)$ is found for the growth rates of convective modes branching from the static state (equation (4)) as long as the amplitudes remain small. Growth rates σ of axisymmetric solutions (wavenumber $m = 0$) can easily be derived as

$$\sigma = -\tfrac{1}{2}(n^2\pi^2 + \lambda_j^2)(1+P)\left\{1 \pm \left[1 - \frac{4P(1-R/R_{0,j,n})}{(1+P)^2}\right]^{\frac{1}{2}}\right\}. \tag{7}$$

In agreement with the nomenclature of Rosenblat, $n = 1, 2, 3, \ldots$ is associated with the number of zeros of the solution in the z-direction, and is called the vertical wavenumber and $j = 1, 2, 3, \ldots$ is the radial wavenumber; λ_j is the jth positive root determined by the condition $J_1(\lambda/2a) = 0$, J_1 is the usual Bessel function of order 1, $a = h/d$ is the aspect ratio and $R_{0,j,n}$ the critical Rayleigh number for the eigensolution (mode) $m = 0, j, n$ obtained by Rosenblat.

In agreement with theory an exponential law for the growth of small-amplitude disturbances is found in the numerical simulations. Dependences of the growth rates on the mesh size and time step are shown in figure 2. It can be seen that the values for σ obtained numerically converge to the exact analytical value with decreasing time step and mesh size, i.e. the finite-difference scheme is consistent with the differential formulation.

Stability boundaries, e.g. critical Rayleigh numbers for the onset of convection

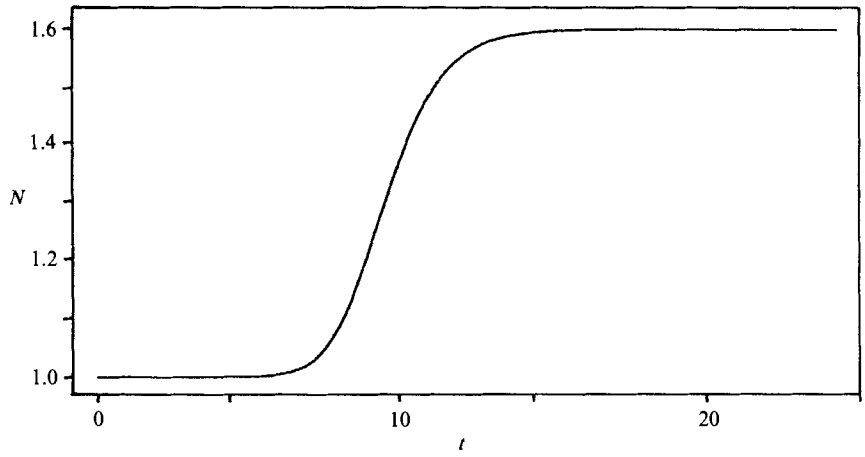

FIGURE 3. Time evolution of the Nusselt number for a shear-free cylinder with $a = 0.2899$ and an adiabatic sidewall; $R = 1000$; $P = 1$.

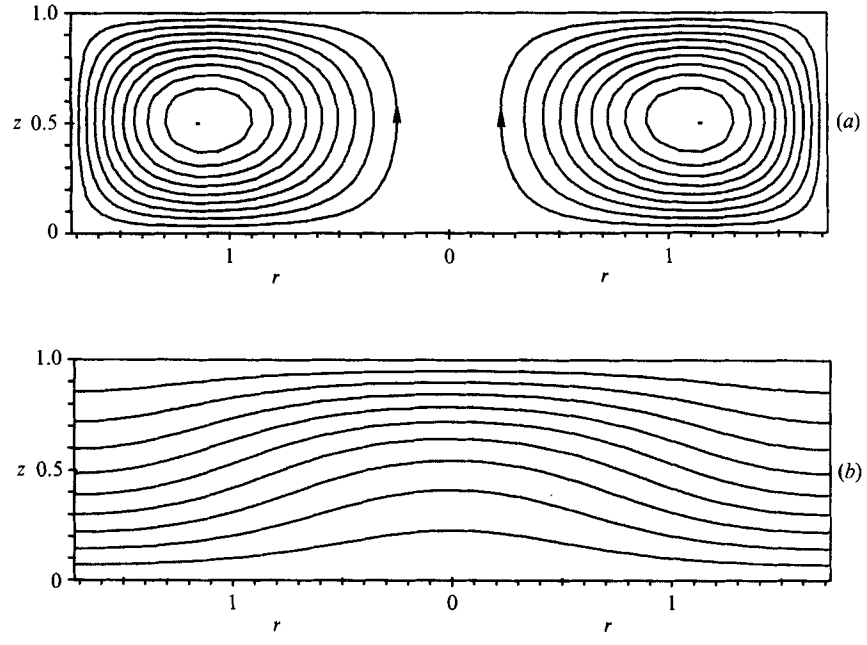

FIGURE 4. (*a*) Streamlines and (*b*) isotherms of axisymmetric convection in a shear-free cylinder for $a = 0.2899$, adiabatic sidewall, $R = 700$ and $P = 1$.

($R_{c,s}$), cannot be directly calculated by means of any numerical scheme. However, the present numerical procedure enables the approximate determination of stability boundaries, as follows. Growth rates σ of small-amplitude convective disturbances are calculated for different values of the Rayleigh number. The critical Rayleigh number for this type of instability is evaluated by extrapolation to $\sigma = 0$. The accuracy of this method is tested by comparison with the analytical result of Rosenblat (1982). Good agreement is obtained, as shown in table 1.

For calculating the amplitude of the convective motion at supercritical Rayleigh numbers the numerical procedure is repeated for a sufficient number of time

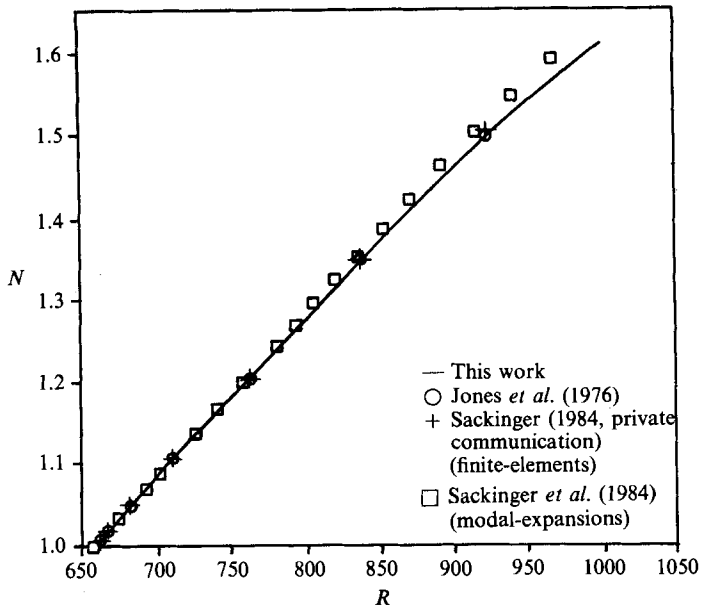

FIGURE 5. Nusselt number versus Rayleigh number for axisymmetric convection in a shear-free cylinder for $a = 0.2899$, adiabatic sidewall and $P = 1$. Comparison between different computational methods.

increments to converge to a steady state. In figure 3 the development of buoyancy convection in a cylinder with shear-free walls is represented by the dimensionless Nusselt number. At $t = 0$ the calculation starts with the static solution (equation (4)). Small-amplitude temperature disturbances ($T' < 0.01$) are added to the static state in order to enhance the convective motion. The calculation is stopped when the relative change of the Nusselt number between two time steps is smaller than 10^{-4}. The stream pattern and temperature distribution of the converged solution is plotted in figure 4. The axisymmetric convection pattern consists of one toroidal roll, in agreement with the prediction of the linear theory of Rosenblat for the aspect ratio $a = 0.2899$†. Two convective toroids (mode $m = 0, j = 2, n = 1$) are predicted by the linear theory for the larger aspect ratio $a = 0.21$. This is also found in the numerical calculation. For the single-roll solution a comparison of the results of different numerical methods is shown in figure 5 by a plot of the Nusselt number versus the Rayleigh number. Good agreement with the numerical results of Jones, Moore & Weiss (1976) and P. A. Sackinger (1984, private communication) is obtained.

4. Steady convective regimes

The aim of the following sections is to study the nonlinear evolution of steady convective regimes in cylindrical containers with rigid walls. The dependence of the convective behaviour on the Rayleigh and Prandtl number and on the boundary and initial conditions is also investigated. Convective flow patterns are calculated for two typical aspect ratios: $a = 0.5$ and $a = 1$, which are below and above the critical aspect ratio $a_{c,3D}$ for the transition from axisymmetric to non-axisymmetric

† According to Rosenblat (1982) this aspect ratio corresponds to the minimum critical Rayleigh number $R_{c,s}(a)$ for the axisymmetric $m = 0, j = 1, n = 1$ mode (one toroidal roll).

Aspect ratio, a	Critical Rayleigh numbers, $R_{c,s}$			
	Numerical $\sigma \to 0$	Charlson & Sani (1971)	Gershuni & Zhukhovitskii (1976)	Buell & Catton (1983)
0.5	2.22×10^3	2.26×10^3	2.25×10^3	2.26×10^3
1	3.61×10^3	4.5×10^3	3.9×10^3	3.8×10^3

TABLE 2. Comparison of critical Rayleigh numbers for the onset of convection in rigid cylinders with adiabatic sidewalls obtained by extrapolation with the results of linear stability theories

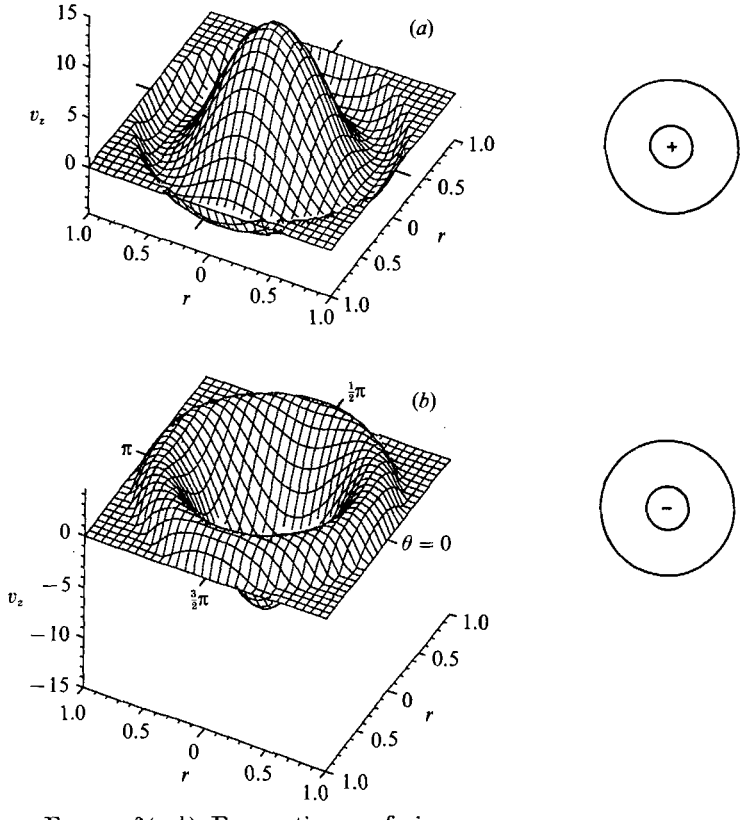

FIGURE 6(a, b). For caption see facing page.

convection predicted by the linear stability theories for the no-slip boundary condition (see §1). According to the investigations of §3.2 a time step $\Delta t = 0.001$ and grids with approximately 20 mesh points in the r-, θ- and z-directions are applied for the numerical simulations.

4.1. *Onset of convection*

Critical Rayleigh numbers $R_{c,s}$ for the onset of (time-independent) convection in rigid cylinders with adiabatic walls are calculated by the extrapolation method described in §3.2. In agreement with linear stability theory, convection sets in with an axisymmetric toroid (mode $m = 0$) for $a = 0.5$ and with a non-axisymmetric single-roll (mode $m = 1$) for $a = 1$. As shown in table 2 the critical Rayleigh numbers obtained in this study are also in good agreement with theory. For the aspect ratio

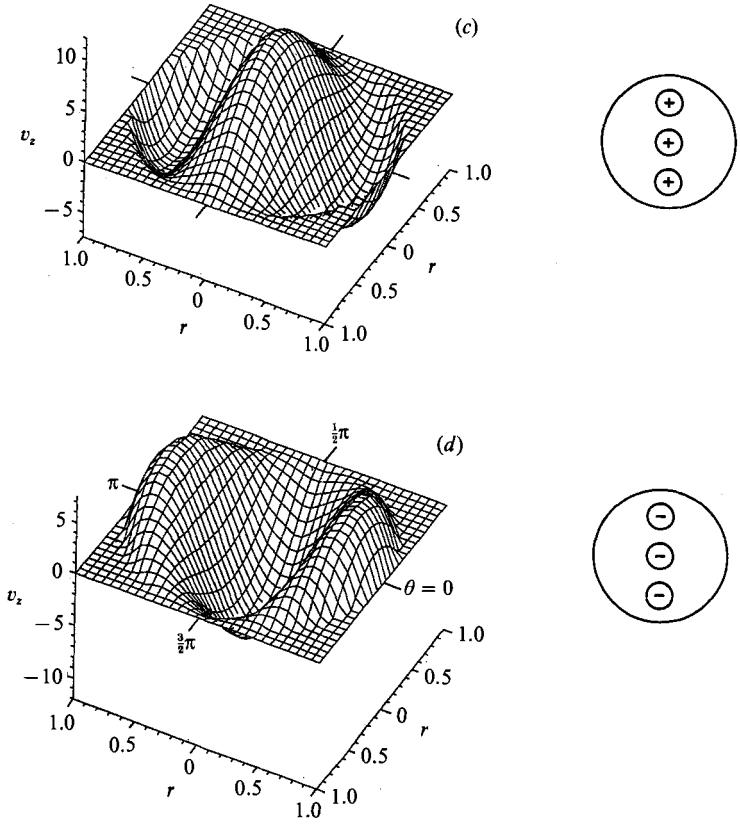

FIGURE 6. Right side: Principle sketch of initial temperature disturbances (T') near the horizontal midplane ($z = 0.5$); ⊕, $T' > 0$ ('hot'); and ⊖, $T' < 0$ ('cold'). Left side: Corresponding steady convection patterns represented by profiles of the vertical velocity component in the horizontal midplane for $a = 0.5$, adiabatic sidewall, $R = 2800$ and $P = 6.7$.

$a = 1$ the numerical calculation seems to confirm the more recent theories of Gershuni & Zhukhovitskii (1976) and Buell & Catton (1983).

4.2. *Dependence of the convective flow on the initial conditions*

For the calculation of supercritical convection the numerical procedure is started from the static state (compare §3.2). Small-amplitude temperature disturbances (T') of various symmetries are added in order to enhance different types of convective flow. Four different types of steady convective flow were found for the supercritical Rayleigh number $R = 2800$, the aspect ratio $a = 0.5$, adiabatic sidewall and $P = 6.7$, corresponding to water. The different flows are represented in figure 6 by a plot of the vertical velocity in the horizontal midplane. The corresponding initial temperature disturbances are sketched on the right-hand side of figure 6. Two equivalent axisymmetric solutions were found, one with upflow and one with downflow in the centre of the container. As pointed out by Liang, Vidal & Acrivos (1969) the system of equations (1) and boundary conditions is invariant under the transformation

$$(z, v_z, T') \rightarrow (1-z, -v_z, -T'),$$

which explains the existence of both downflow and upflow solutions. The Nusselt numbers and flow velocities of the axisymmetric solution are in good agreement with

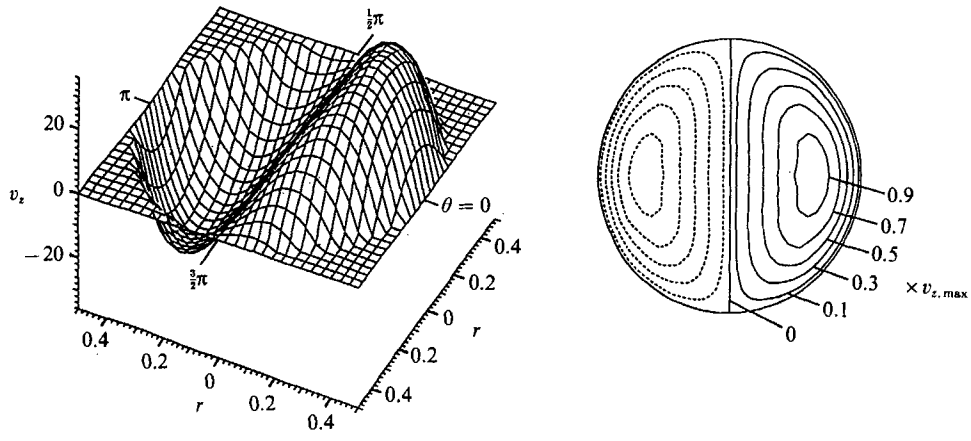

FIGURE 7. Profile of the vertical velocity component and corresponding isotaches in the horizontal midplane ($z = 0.5$) for $a = 1$, adiabatic sidewall, $R = 17\,500$ and $P = 6.7$.

two-dimensional calculations of Liang *et al.* (1969) and Yamaguchi, Chang & Brown (1984). These two types of convection can also be established experimentally, as demonstrated by Müller, Neumann & Weber (1984), who obtained upflow for sidewalls with low thermal conductivity by heating the fluid from below, and downflow by cooling it from above. The non-axisymmetric flow consists of two parallel roll cells with upflow (figure 6*c*) or downflow (figure 6*d*) in the centre. These different types of convection are also predicted by the linear stability theories (e.g. Charlson & Sani 1971), denoted by the mode number $m = 0$ for the axisymmetric and $m = 2$ for the non-axisymmetric two-roll solution. As already shown in §4.1 convection sets in with the axisymmetric mode $m = 0$ for the aspect ratio $a = 0.5$. At the supercritical Rayleigh number of 2800 the linear stability curves of both the $m = 0$ and the $m = 2$ modes are exceeded, which can explain our numerical predictions of convective behaviour. Since the ordering of these linear stability curves does not change in the vicinity of the aspect ratio $a = 0.5$, the above results should not be very sensitive to aspect ratio.

For the aspect ratio $a = 1$ only one stable solution is found, consisting of a single non-axisymmetric roll cell. Different types of temperature disturbances, including random temperature distributions, were applied. The only stable solution corresponds to the mode $m = 1$ predicted by the linear stability theories for aspect ratios $a > 0.58 \pm 0.03$ (adiabatic sidewall) or $a > 0.72 \pm 0.07$ (ideal conducting sidewall). As shown in the plot of the vertical velocity profile in figure 7 the fluid is ascending at one side and descending at the other side of the cylindrical container. With increasing Rayleigh number, i.e. increasing convective momentum transport, the roll becomes more inclined and small counter-rotating eddies arise. This is demonstrated in figure 8 by a plot of the stream pattern in the symmetry plane $\theta = 0, \pi$ which is perpendicular to the axis of the roll. The orientation of the roll in the $\theta = 0, \pi$ plane is given by the initial temperature distribution. The plot of the stream pattern in the plane $\theta = \frac{1}{2}\pi, \frac{3}{2}\pi$ shows that a secondary flow consisting of four symmetric rolls is superimposed. As demonstrated in figure 11 the amplitude of the secondary flow (curve *d*) is much smaller than that of the fundamental single-roll mode (curve *c*). It can be further shown that radial temperature differences aligned with the single-roll mode give rise to the above secondary flow (Neumann 1986). Such a stream pattern

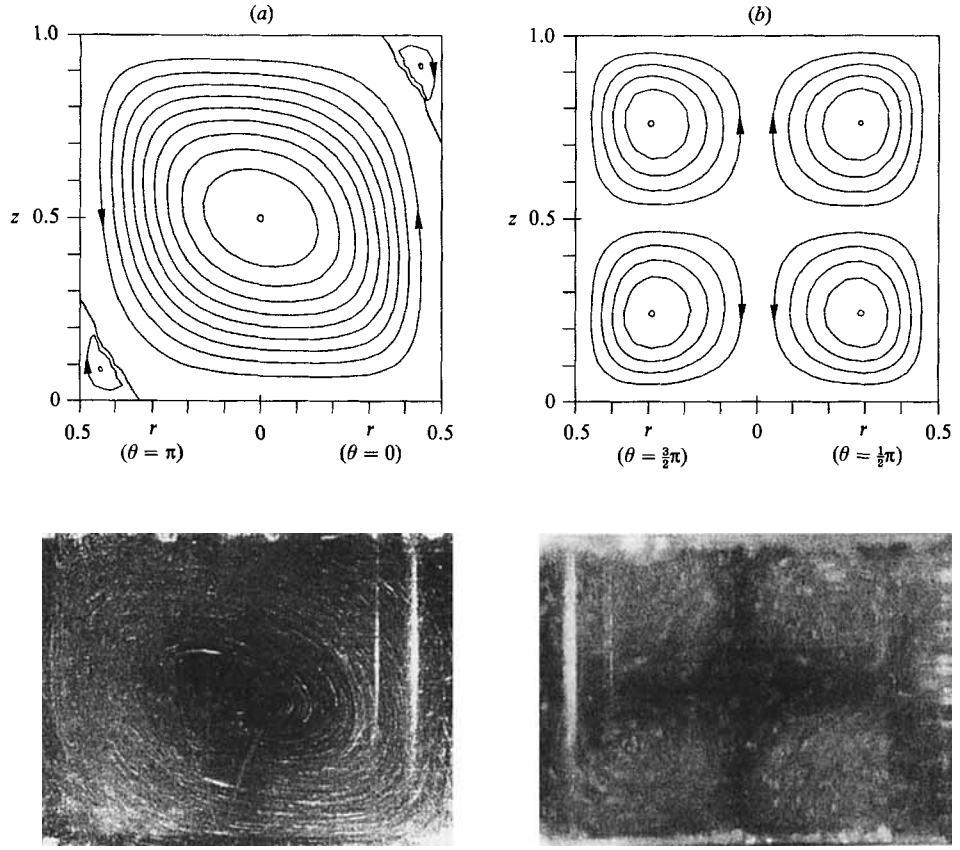

FIGURE 8. Stream pattern in two perpendicular axial sections (*a*) $\theta = 0, \pi$ and (*b*) $\theta = \frac{1}{2}\pi, \frac{3}{2}\pi$ for $a = 1$, adiabatic sidewall, $R = 5 \times 10^4$ and $P = 6.7$ (H_2O). Comparison of the numerical results with experimental flow patterns obtained by the light cut technique (Müller *et al.* 1984).

was also obtained in the numerical studies of Crespo *et al.* (1987) and can be observed in the experimental results of Müller *et al.* (1984) as shown in figure 8.

4.3. *Flow transitions at supercritical Rayleigh numbers*

As observed experimentally (Müller *et al.* 1984) a transition from axisymmetric to three-dimensional convection should evolve for low aspect ratios when the Rayleigh number exceeds a critical value ($R_{c,3D}$). The critical Rayleigh number $R_{c,3D}$ is determined by calculating the growth rates $\sigma(R)$ of three-dimensional disturbances (compare §3.2). For the aspect ratio $a = 0.5$, adiabatic sidewall, and Prandtl number $P = 0.02$, a critical value of $R_{c,3D} = 2525$ is obtained by the present extrapolation method. If R exceeds this critical number the axisymmetric solution (mode $m = 0$) is unstable and bifurcates to the stable non-axisymmetric solution consisting of two parallel roll cells (mode $m = 2$). It should be noted that this bifurcation consists of a direct (not oscillatory) transition from steady axisymmetric to steady non-axisymmetric convection. As already stated in §4.2 such behaviour should be relatively insensitive to aspect ratio. The predicted flow pattern, consisting of two parallel roll cells, has been observed experimentally in the Rayleigh–Bénard

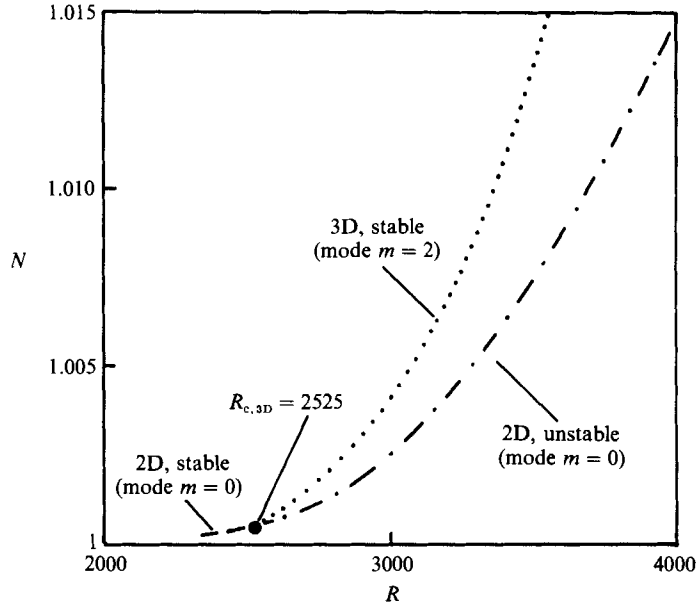

FIGURE 9. Bifurcation from steady axisymmetric (mode $m = 0$) to steady non-axisymmetric (mode $m = 2$) convection represented by a plot of the Nusselt number versus the Rayleigh number for $P = 0.02$, $a = 0.5$ and an adiabatic sidewall. Beyond the critical Rayleigh number $R_{c,3D} = 2525$ the axisymmetric solution is unstable to three-dimensional disturbances.

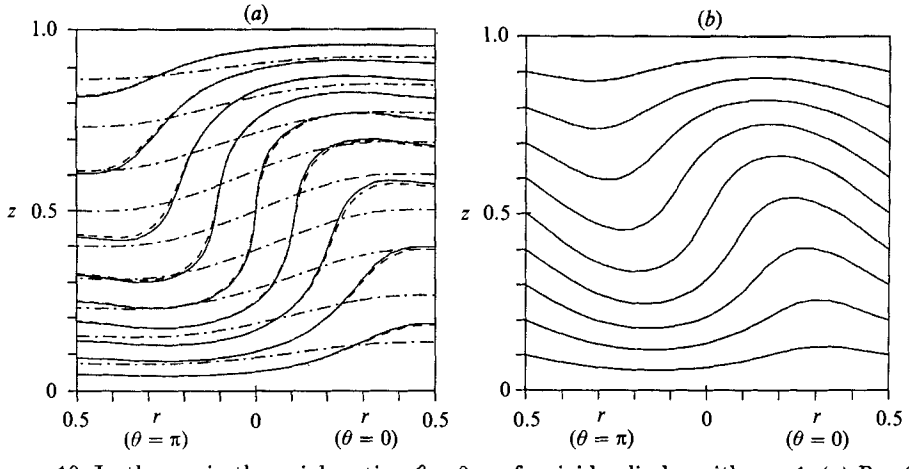

FIGURE 10. Isotherms in the axial section $\theta = 0, \pi$ of a rigid cylinder with $a = 1$. (*a*) $R = 6000$, an adiabatic sidewall and three different Prandtl numbers are assumed.: $P = 6.7$ (——), $P = 1$ (– – – – – –) and $P = 0.02$ (–·–·–·–). (*b*) $R = 10000$, an ideal conducting sidewall and $P = 6.7$ are assumed.

experiments of Fauve & Libchaber (1984) for the low-Prandtl-number fluid mercury ($P = 0.03$).

The bifurcation to the non-axisymmetric solution is shown in figure 9 by a plot of N versus R. For the same aspect ratio ($a = 0.5$) but using a Prandtl number $P = 1$, a critical Rayleigh number $R_{c,3D} = 4100$ is obtained.

For the aspect ratio $a = 1$ (mode $m = 1$, see figures 7, 8) no flow transition is found within the investigated range of $R (R \leqslant 5 \times 10^4)$.

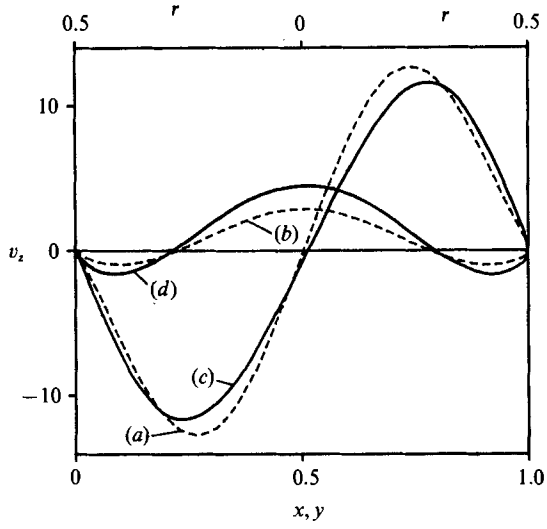

FIGURE 11. Vertical velocity profiles computed in this study for a cylinder with $a = 1$ and $P = 6.7$ and by K. R. Kirchartz (1984, private communication) for a cube and $P = 0.71$. Ideal conducting walls and $R = 10000$ are assumed for both geometries. Cylinder (——): v_z versus r at $z = 0.5$, $\theta = 0, \pi$ (curve c) and at $z = 0.75$, $\theta = \frac{1}{2}\pi, \frac{3}{2}\pi$ (curve d). Cube with length $0 \leqslant x \leqslant 1$, width $0 \leqslant y \leqslant 1$ and height $0 \leqslant z \leqslant 1$ (– – – –): v_z versus x at $y = 0.5$, $z = 0.5$ (curve a) and v_z versus y at $x = 0.5$, $z = 0.75$ (curve b).

4.4. *Dependence of the convective flow on the Prandtl number and the thermal boundary conditions*

The dependence of the symmetry and structure of the flow on the Prandtl number and the thermal boundary condition is investigated for the aspect ratio $a = 1$. In the range $0.02 \leqslant P \leqslant 6.7$ and for the two cases of adiabatic and ideal conducting sidewalls, qualitatively similar flow pattern are obtained. For both cases the solution consists of a non-axisymmetric basic roll cell with a small-amplitude secondary flow (see §4.2) superimposed. The qualitative agreement is demonstrated by a plot of the temperature field in the $\theta = 0, \pi$ symmetry plane (figure 10). The isotherms are found to be flatter for $P = 0.02$ compared with $P = 1$ and 6.7, which can be attributed to the high thermal conductivity of small-Prandtl-number fluids. The temperature and velocity fields obtained for $P = 1$ and 6.7 are almost the same. This behaviour is in agreement with theoretical results of Clever & Busse (1981), who show that convective flow in the case of moderate R is nearly independent of the Prandtl number for $P \geqslant 1$.

4.5. *Dependence of the convective flow on the geometry of the container*

The influence of container geometry on the flow has been studied by comparing flow patterns in cylindrical containers with those obtained for cubic boxes (Kirchartz & Oertel 1988). Figure 11 shows a comparison of vertical velocity profiles in a cylinder of aspect ratio $a = 1$ with the corresponding profiles computed for a cube. The amplitude of the fundamental single-roll mode with upflow at one side of the container and downflow at the other side (compare figure 8*a*) is represented by curves (*a*) and (*c*), whereas the secondary flow (compare figure 8*b*) is represented by curves (*b*) and (*d*). The configuration and amplitude of the flow velocity are quite similar in containers with circular and square cross-sections.

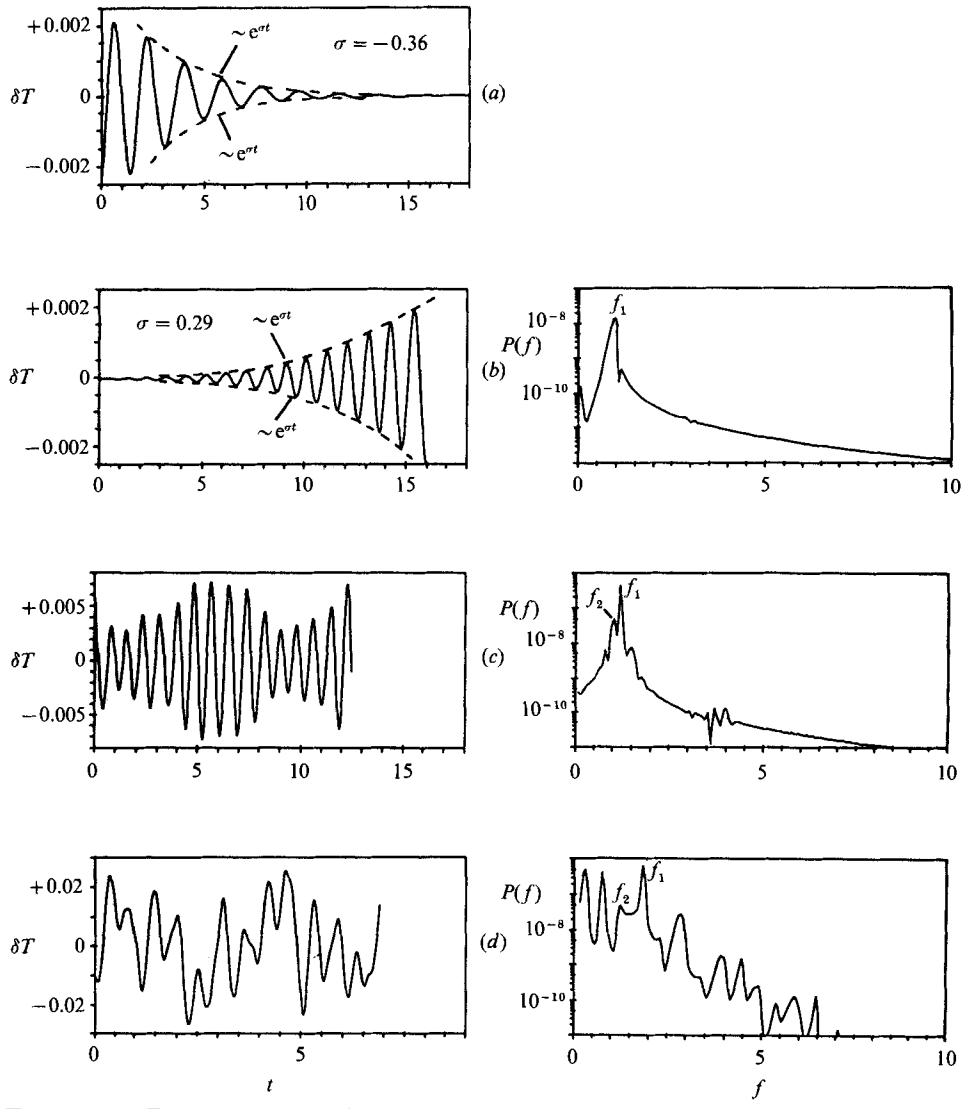

FIGURE 12. Time evolution of a computed temperature difference $\delta T = T(r = 1, \theta = 0, z = 0.5) - T(r = 1, \theta = \pi, z = 0.5)$ and corresponding power spectra at $P = 0.02$, $a = 0.5$, an adiabatic sidewall and various Rayleigh numbers: (*a*) $R = 4000$; (*b*) $R = 5000$; (*c*) $R = 6000$; (*d*) $R = 8000$.

5. Time-dependent convection

Transitions from steady to time-dependent convection are studied for the Prandtl number 0.02, which corresponds to most of the liquid metals (e.g. Ga) of current interest for bulk semiconductor crystal growth. The critical Rayleigh number $R_{c,t}$ for the onset of oscillatory instability is determined indirectly by nonlinear time-dependent calculations. Typically for Rayleigh–Bénard configurations the steady solution becomes unstable with respect to time-periodic disturbances if the Rayleigh number exceeds a critical number. Growth exponents $\hat{\sigma} = \sigma + i\omega$ of time-dependent disturbances are computed for the two-roll solution (mode $m = 2$, see §4.3) obtained for the aspect ratio $a = 0.5$, $P = 0.02$ and $R > 2525$. Round-off errors of the

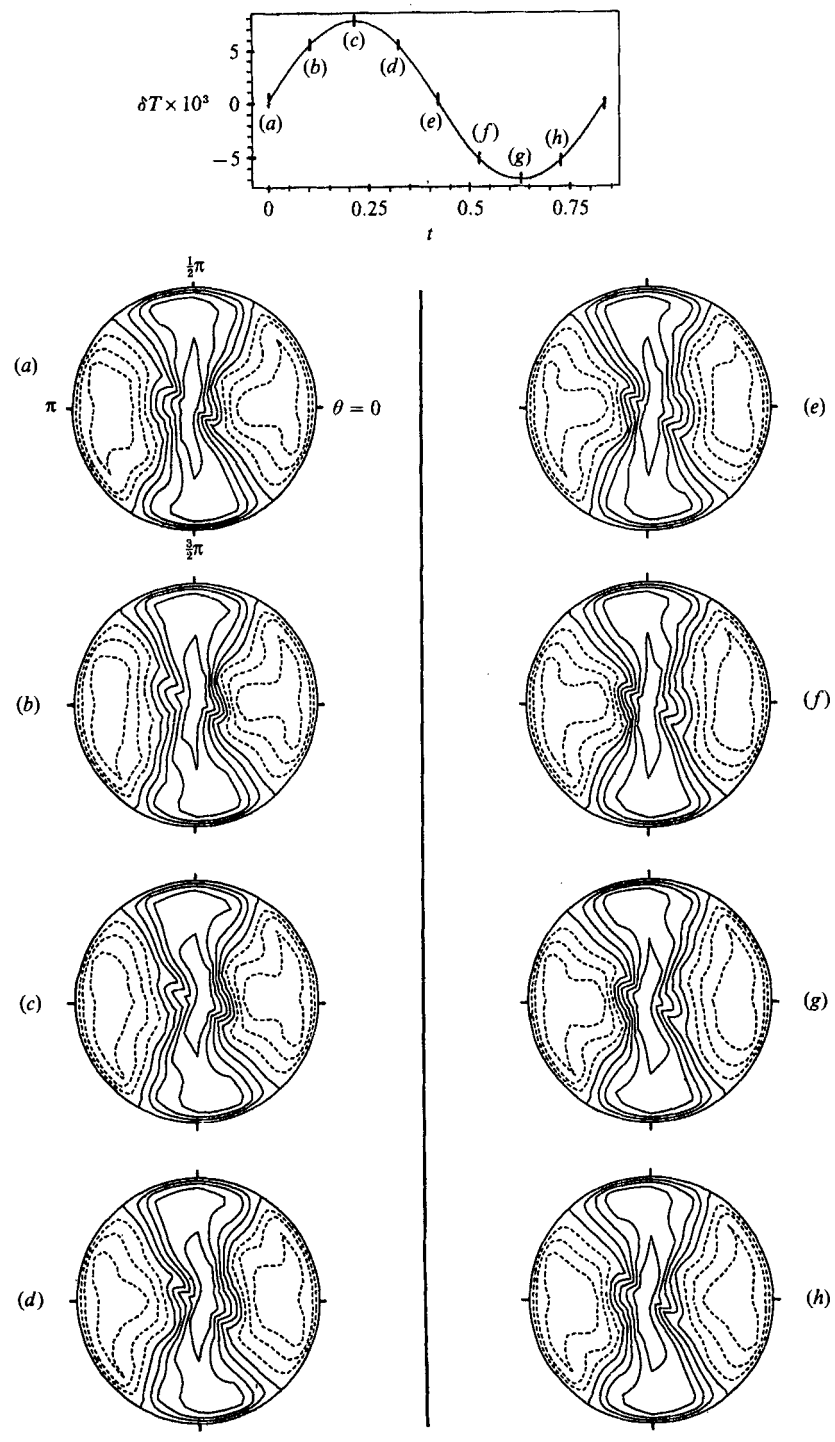

FIGURE 13. Isotaches of the vertical velocity component in the horizontal midplane during one oscillation period for $R = 6000$, $P = 0.02$ and $a = 0.5$. Times are denoted by (a–h) in the plot of δT versus t. Upflow ($v_z \geqslant 0$) is represented by solid lines and downflow ($v_z < 0$) by broken ones.

Author	Fluid	P	R	Frequency $f_1^{\mathrm{dim.}}$ (Hz)	Dimensionless frequency $f_1 = f_1^{\mathrm{dim}}/(\kappa/h^2)$
This work, numerical	—	0.02	5000	—	0.9
	—	0.02	6000	—	1.2
		0.02	8000	—	1.8
Weber (1988), experimental	Ga	0.02	8000	0.09	2.0
Fauve & Libchaber (1984), experimental	Hg	0.03	7500	≈ 0.1	≈ 2

TABLE 3. Oscillation frequencies of time-dependent thermal convection in vertical cylinders of aspect ratio $a = 0.5$

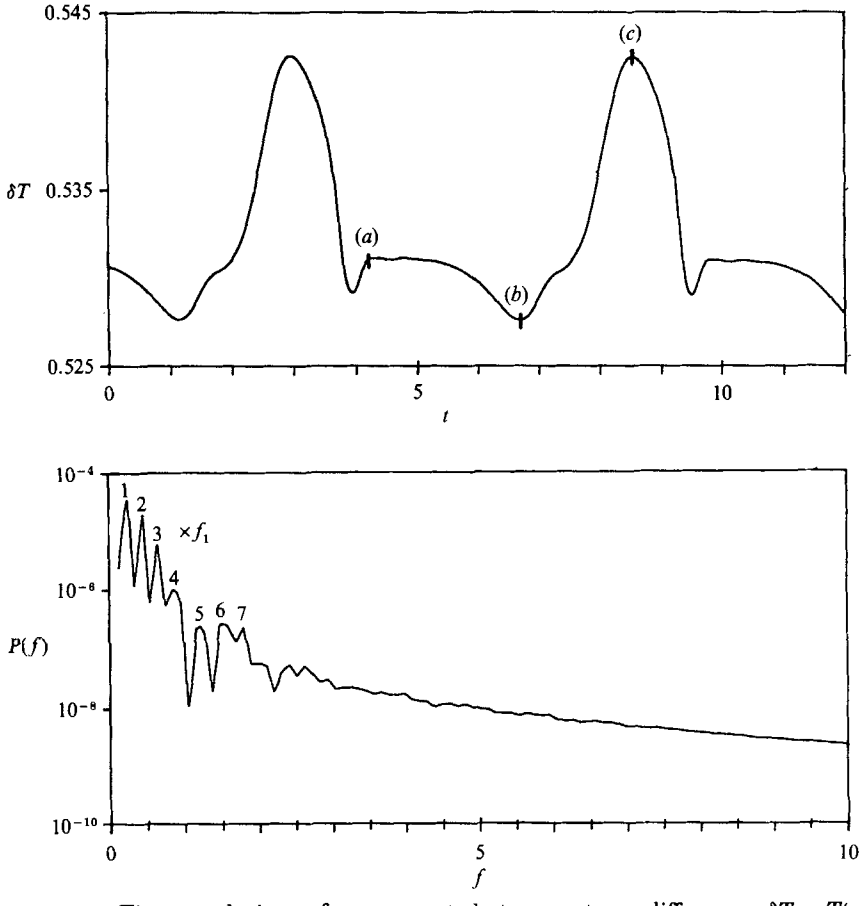

FIGURE 14. Time evolution of a computed temperature difference $\delta T = T(r = 0.5, \theta = 0, z = 0.5) - T(r = 0.5, \theta = \pi, z = 0.5)$ and the corresponding power spectrum for $R = 16000, P = 0.02$, $a = 1$ and an adiabatic sidewall.

numerical simulation are sufficient to initiate the oscillatory instability. Since the oscillatory disturbances require a finite time to develop, a quasi-steady state can be calculated before the oscillation sets in. An example of the evolution of time-dependent disturbances branching from the quasi-steady state mode ($m = 2$) is

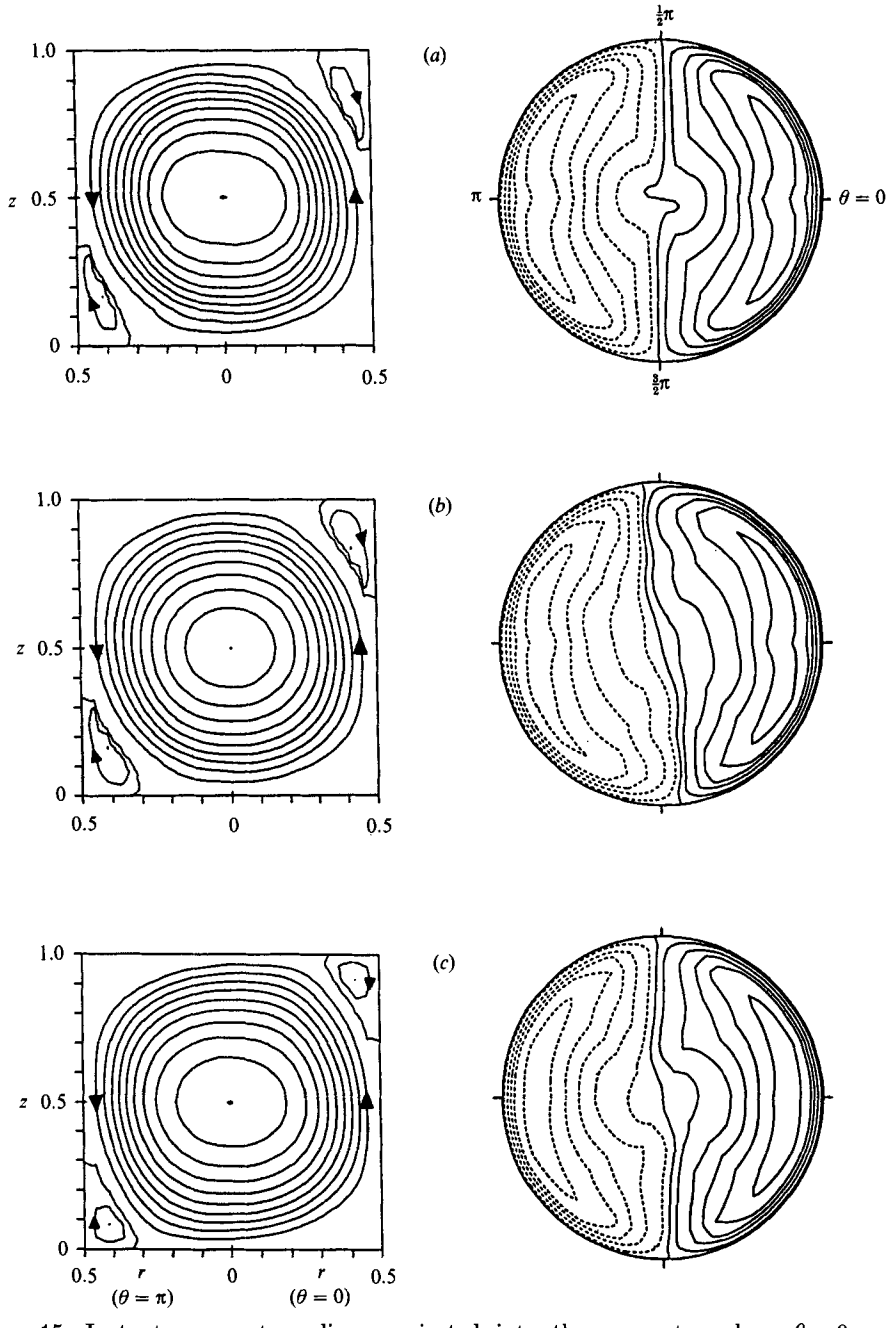

FIGURE 15. Instantaneous streamlines projected into the symmetry plane $\theta = 0$, π of the unperturbed steady solution (compare figures 7, 8) and isotaches of the vertical velocity component in the horizontal midplane ($z = 0.5$) for $R = 16000$, $P = 0.02$ and $a = 1$. (*a*) $t = 4.5$; (*b*) $t = 6.7$; (*c*) $t = 8.5$ (*a*, *b*, *c* shown on figure 14).

shown in figure 12(*b*). The oscillation shown in figure 12(*b*) grows exponentially with $\sigma = 0.29$. Decreasing the Rayleigh number to $R = 4000$ (figure 12*a*) damps the oscillation to $\sigma = -0.36$. The critical Rayleigh number $R_{c,t}$ can be calculated approximately by linear interpolation to $\sigma = 0$, resulting in $R_{c,t} = 4550$ for the

transition from non-axisymmetric steady state (mode $m = 2$) to the time-dependent solution for $a = 0.5$, $P = 0.02$ and an adiabatic sidewall.

For $R = 6000$ (figure 12*c*) a second oscillatory mode of frequency f_2 close to the fundamental frequency f_1 appears. The change of the spatial structure of the time-dependent flow field can be seen in a representation of the velocity distributions during one oscillation (figure 13) and consists of only slight deformations. This low-Prandtl-number solution is completely different from oscillatory convection observed in gases with $P \approx 1$ (Mitchell & Quinn 1966). Oscillations in gases consist of rotations (e.g. the symmetry plane of the two-roll mode) around the axis of the cylinder.

At a Rayleigh number of 8000 (figure 12*d*), oscillations of lower frequency are superimposed and the behaviour becomes non-periodic. The fundamental frequency f_1 is compared with the results of experimental investigations in table 3, giving a good agreement between the numerical calculations and the temperature measurements.

For the aspect ratio $a = 1$ (mode $m = 1$) time-dependent convection sets in with strongly non-harmonic temperature fluctuations (figure 14). The fundamental frequency of this oscillatory flow is relatively low (compare figures 12 and 14). The critical Rayleigh number $R_{c,t} = 1.5 \times 10^4$ is obtained for $a = 1$, $P = 0.02$ and an adiabatic sidewall. In figure 15 the flow pattern is shown at three different times during one cycle of the periodic fluctuation (denoted by *a*, *b* and *c* in figure 14). Again the structure of the flow does not change substantially during the oscillation. For a CRAY-1 computer a run-time of 5800 CPU-seconds was necessary for the calculation of the two periods of oscillation shown in figure 14. A time step of 0.001 was used, corresponding to a typical value of about $\frac{1}{2}$ CPU-second per time step for a numerical grid with 6912 mesh points (i.e. 16 radial, 18 azimuthal, and 24 vertical mesh points). The occurrence of oscillations very similar to the above numerical predictions has also been observed in crystal growth experiments (Kyr 1978). The measured frequency of $f_1 \approx 0.15$ ($f_1^{\mathrm{dim}} \approx 0.025$ Hz) is also in good agreement with the numerical value of $f_1 = 0.18$.

6. Discussion

Buoyancy-driven convection in vertical cylinders heated from below has been analysed with a fully three-dimensional and time-dependent numerical scheme.

Predictions of the onset of convective motion show good agreement with the results of linear stability theories, in particular the critical Rayleigh numbers ($R_{c,s}$) and the structure and stability of the first convective instability.

The nonlinear numerical analysis of convection in rigid cylinders clearly shows that stable axisymmetric solutions are not only limited to flat cylindrical enclosures but are also further restricted to small Rayleigh numbers. The value of R for the transition from axisymmetric to non-axisymmetric convection is strongly influenced by nonlinear interactions. For the small Prandtl number 0.02 the nonlinear behaviour is more pronounced, and a relatively low critical Rayleigh number $R_{c,3D} = 2525$ is found for the transition to the non-axisymmetric flow pattern at an aspect ratio $a = 0.5$. For $P = 1$ the transition occurs at a higher critical Rayleigh number, $R_{c,3D} = 4100$. It is interesting to note that both axisymmetric and non-axisymmetric solutions could be found for an intermediate Rayleigh number of 2800, depending on the initial conditions. No significant dependence on the Prandtl number is found for $P \geqslant 1$, in agreement with nonlinear calculations of Jones *et al.* (1976) and Clever & Busse (1981).

The transition from laminar to oscillatory convection was determined from nonlinear, time-dependent calculations for the Prandtl number 0.02. For the onset of time-dependent convection the ratio $R_{c,t}/R_{c,s} = 2.0$ was obtained for the aspect ratio $a = 0.5$ and $R_{c,t}/R_{c,s} = 4.1$ for $a = 1$. For $P = 6.7$ and $a = 1$ steady convection was found within the whole investigated range up to $R = 5 \times 10^4$, i.e. it can be assumed that $R_{c,t}/R_{c,s} > 13.8$. The above result, i.e. that the critical Rayleigh number for the onset of time-dependent convection decreases strongly for small Prandtl numbers, is well known and was also found in the experiments of Krishnamurti (1973), who investigated the onset of unsteady Rayleigh–Bénard convection in fluid layers of large horizontal extent. For liquid mercury with $P = 0.025$ Krishnamurti obtained the critical number $R_{c,t}/R_{c,s} = 1.4$. The higher stability of laminar convection calculated in this work for the confined fluids can be attributed to the damping influence of the lateral wall.

Since oscillatory convection must in general be avoided during crystal growth (Müller 1988), the determination of oscillatory regimes and their dependence on the geometry, thermal boundary conditions, etc. is important for the optimization of various growth processes. As shown in §5, and in more detail by Müller *et al.* (1984) and Neumann (1986), the results obtained for the idealized model presented in this study are in good agreement with those obtained from vertical crystal growth experiments as long as convection is controlled by destabilizing vertical temperature gradients.

I would like to express my thanks to Professor G. Müller, who initiated this work, for his encouragement and helpful discussions throughout this work. I would also like to thank Professor R. A. Brown and Dr G. Scheuerer for valuable advice. This work was supported by the German Bundesministerium für Forschung und Technologie under Grant No. 01 QV 8522 9.

REFERENCES

Bénard, H. 1900 Les tourbillons cellulaire dans nappe liquide transportant de la chaleur pur convections en règime permanent. *Rev. Gen. Sci. Pures Appl. Bull. Assoc.* **11**, 1261–1271, 1309–1328.

Buell, J. C. & Catton, I. 1983 The effect of wall conduction on the stability of a fluid in a right circular cylinder heated from below. *J. Heat Transfer* **105**, 255–260.

Catton, I. & Edwards, D. K. 1967 Effect of side walls on natural convection between horizontal plates heated from below. *Trans. ASME* C: *J. Heat Transfer* **89**, 295–299.

Chandrasekhar, R. S. 1961 *Hydromagnetic and Hydrodynamic Stability.* Oxford University Press.

Charlson, G. S. & Sani, R. L. 1971 On thermoconvective instability in a bounded cylindrical fluid layer. *Intl J. Heat Mass Transfer* **14**, 2157–2160.

Clever, R. M. & Busse, F. H. 1981 Low-Prandtl-number convection in a layer heated from below. *J. Fluid Mech.* **102**, 61–74.

Crespo, E., Bontoux, P., Smutek, C., Roux, B., Harding, G., Sani, R. L. & Rosenberger, F. 1987 Three-dimensional simulations of convective regimes in cylindrical ampoules. Comparisons with theoretical analysis and experiments. *Proc. 6th Europ. Symp. on Material Sciences under Microgravity Conditions, Bordeaux, France, 2–5 Dec. 1986* (ESA SP-256, February 1987).

Douglas, J. & Gunn, J. 1964 A general formulation of Alternating Direction Methods. *Numer. Maths* **6**, 428–453.

Fauve, S. & Libchaber, A. 1984 Rayleigh–Bénard experiment in a low Prandtl number fluid, mercury. In *Chaos and Order in Nature* (ed. H. Haken), pp. 25–35. Springer.

GERSHUNI, G. Z. & ZHUKHOVITSKII, E. M. 1976 *Convective Stability of Incompressible Fluids.* Keterpress Enterprises.

HARLOW, F. H. & WELCH, J. E. 1965 Numerical calculation of time-dependent viscous incompressible flow of fluid with free surfaces. *Phys. Fluids* **8**, 2183–2189.

JONES, C. A., MOORE, D. R. & WEISS, N. O. 1976 Axisymmetric convection in a cylinder. *J. Fluid Mech.* **73**, 353–388.

KIRCHARTZ, K. R. & OERTEL, H. 1988 Three-dimensional convection in rectangular boxes. *J. Fluid Mech.* **192**, 249–286.

KRISHNAMURTI, R. 1973 Some further studies on the transition to turbulent convection. *J. Fluid Mech.* **60**, 285–303.

KYR, P. 1978 Konvektion in Schmelzen mit kleiner Prandtlzahl bei Vielfachen der Erdbeschleunigung. Diplomarbeit, Universität Erlangen, FRG.

LIANG, S. F., VIDAL, A. & ACRIVOS, A. 1969 Buoyancy-driven convection in cylindrical geometries. *J. Fluid Mech.* **36**, 239–256.

MITCHELL, W. T. & QUINN, J. A. 1966 Thermal convection in a completely confined fluid layer. *AIChE J.* **12**, 1116–1124.

MÜLLER, G. 1988 *Crystals – Growth, Properties and Applications*, Vol. 12: *Convection and Inhomogeneities in Crystal Growth from the Melt.* Springer.

MÜLLER, G., NEUMANN, G. & WEBER, W. 1984 Natural convection in vertical Bridgman configurations. *J. Cryst. Growth* **70**, 78–93.

NEUMANN, G. 1986 Berechnung der thermischen Auftriebskonvektion in Modellsystemen zur Kristallzüchtung. Dissertation, Universität Erlangen, FRG.

PATANKAR, S. V. 1980 *Numerical Heat Transfer and Fluid Flow.* Hemisphere.

PIACSEK, S. A. & WILLIAMS, G. P. 1970 Conservation properties of convection difference schemes. *J. Comp. Phys.* **6**, 392–405.

ROSENBLAT, S. 1982 Thermal convection in a vertical circular cylinder. *J. Fluid Mech.* **122**, 395–410.

SACKINGER, P. A., BROWN, R. A., NEUMANN, G. & MÜLLER, G. 1984 Eigenfunction expansions for nonlinear convection in a vertical cylinder heated from below. *Bull. Am. Phys. Soc.* **29**, 1523.

SCHLÜTER, A., LORTZ, D. & BUSSE, F. 1965 On the stability of steady finite amplitude convection. *J. Fluid Mech.* **23**, 129–144.

WEBER, W. 1988 Untersuchung der thermischen Auftriebskonvektion in Modellsystemen zur Kristallzüchtung bei normaler und erhöhter Schwerkraft. Dissertation, Universität Erlangen, FRG.

WILLIAMS, G. P. 1969 Numerical integration of the three-dimensional Navier–Stokes equations for incompressible flow. *J. Fluid Mech.* **37**, 727–750.

YAMAGUCHI, Y., CHANG, C. J. & BROWN, R. A. 1984 Multiple buoyancy-driven flows in a vertical cylinder heated from below. *Phil. Trans. R. Soc. Lond.* A **312**, 519–552.

ZIEREP, J. 1963 Zur Theorie der Zellularkonvektion: Zellular-Konvektionsströmungen in Gefäßen endlicher horizontaler Ausdehnung. *Beitr. Z. Phys. Atmos.* **36**, 70–76.